



Spatiotemporal characteristics of extreme droughts and their association with sea surface temperature over the Cauvery River basin, India

Pravat Jena¹ · K. S. Kasiviswanathan² · Sarita Azad¹

Received: 4 April 2020 / Accepted: 27 August 2020 / Published online: 5 September 2020
© Springer Nature B.V. 2020

Abstract

Drought is a function of time as well as climate variables such as temperature and precipitation. The process of drought forming is slow, and it manifests at different time scales, which adversely affects the economy of a country. The identification and characterization of droughts at various spatiotemporal scales are of great importance. It helps in the planning and management of water resources, policymaking, and agribusiness industries. In the present paper, the Cauvery River basin is chosen as a study area to analyze the changes in the frequency distribution of extreme droughts and duration, with the combined effect of evapotranspiration and rainfall. The drought indices such as Standard Precipitation Index (SPI) and Standard Precipitation Evapotranspiration Index (SPEI) are implemented on monthly rainfall data and potential evapotranspiration of resolution $0.25^\circ \times 0.25^\circ$ long./lat. for the period 1931–2010. The results reveal that the frequency of the extreme droughts over the basin has significantly increased over the post-era of global warming. The increased rate of extreme droughts is particularly evident in downstream of the basin, mainly due to the increase in temperature and deficit rainfall. Further, the implementation of continuous wavelet transform reveals that SPI at 3-(SPI-3) and 12-(SPI-12) month scale are associated with extended reconstruction of sea surface temperature (ERSST) in anti-phase and in-phase, respectively. It is concluded that the in-phase association of SPI-12 and ERSST enhances the drought situation compared to the anti-phase link of SPI-3 and ERSST.

Keywords SPI · SPEI · River basin · Wavelet · TBO · Drought intensity · Extreme drought

✉ Sarita Azad
sarita@iitmandi.ac.in

¹ School of Basic Sciences, Indian Institute of Technology Mandi, Kamand 175 005, India

² Department of Water Resources Development and Management, Indian Institute of Technology Roorkee, Roorkee 247 667, India

1 Introduction

The hydrological cycle is known to be very susceptible to projected climate changes. It has been shown in several studies that global warming has affected precipitation patterns (Fowler and Hennessy 1995; Xie et al. 2010), and more frequent floods, droughts, and rainstorms have been witnessed due to extreme weather conditions (Zhang et al. 2008). Flooding is, in general, an immediate response of catchment. In contrast, droughts are a slow and long-term process mainly resulting from the change in meteorological variables such as precipitation and temperature. Droughts occur at different time scales, which affect large regions directly or indirectly and cause significant damages mainly to agricultural activities and loss of livelihood (Vasiliades et al. 2011; Narasimhan and Srinivasan 2005). Since 1967, 50% of the world population has been affected by the impact of droughts (Obasi 1994) and it accounts for a significant portion of agricultural land (USDA 1994). It has been shown that 75% of the agricultural land lies in the river basin across the world, which plays the lifeline of entire living beings (USDA 1994).

India's economy is mainly dependent on agricultural products, which contributes to an 18.1% share of the country's gross domestic product (GDP), and it creates approximately 52% of employment opportunities (Arjun 2013). The agriculture in India mainly depends on monsoon rainfall which is generally managed by several storage/diversion schemes (i.e., through various hydraulic structures). Thus, any deficit of the rain might cause an impact on the overall agricultural productivity. Therefore, there is a need to understand the changing frequency of dryness through integrated water resource management at the river basin scale.

There are several classifications of droughts such as meteorological (Hisdal and Tallaksen 2003; Mishra and Singh 2010), agricultural (Mishra and Singh 2010), and hydrological (Hisdal and Tallaksen 2003; Dracup et al. 1980; Sen 1980). In general, a drought year is defined as the anomaly of average rainfall fall below 10% of its long-term mean over the region of interest (Kumar et al. 2013). There are many functions which have been developed to monitor the droughts such as the Reconnaissance Drought Index (RDI) (Tsakiris et al. 2007), the Drought Severity Index (DSI) (Pandey et al., 2008) and the Streamflow Drought Index (SDI) (Nalbantis and Tsakiris 2009). However, the Standard Precipitation Index (SPI), developed by McKee et al. (1993), is being recommended by World Meteorological Organization (WMO) and implemented by many researchers (Guttman 1998; Pai et al. 2017). The main drawback of SPI has been that it uses rainfall data mainly, and other critical climate variables are not considered in its calculations. Moreover, it has been noted that along with precipitation, other climate variables such as temperature also play a vital role to intensify the drought condition. During the last 150 years, the global average temperature increased by 2–5 °C (Gao et al. 2017; Jones and Moberg 2003) and coupled climate change models predicted an increase of 4 °C during the 21st century (IPCC 2007). A recent study concluded that the simultaneous rise in temperature and decrease in precipitation might result in a deficiency of soil moisture (Logan et al. 2010). For this reason, the importance of analyzing trends in the temperature toward water resources applications and drought analysis has already been proven in previous studies (Nicholls 2004; Cai and Cowan 2008; Gerten et al. 2008; Lorenzo-Lacruz et al. 2010). The combined effect of precipitation and temperature can be studied through a function called the Palmer Drought Severity Index (PDSI) (Palmer 1965). However, the functionality of PDSI depends on fixed time scales, and it fails when the time scale varies. This difficulty can be avoided by the use of another drought index namely, the Standardized Precipitation Evapotranspiration Index

(SPEI) proposed by Begueria et al. (2010), Vicente-Serrano et al. (2010a), and Vicente-Serrano et al. (2010b) to quantify the drought conditions considering both these climate variables.

In general, the droughts analyses, including the intensity, duration, and frequency using both SPI and SPEI indices, have been investigated. Also, the periodical behavior of moderate drought events is analyzed using the wavelet transform functions. However, the variability of drought indices over time and their interaction with the extended reconstruction of sea surface temperature (ERSST) have not been analyzed at the river basin scale, especially in India. It may be noted that among several rivers in India, the Cauvery River has its vital significance in the peninsular region mainly because of the perennial flow. This river supports the irrigation practices since ancient kingdoms. In the last century, besides irrigation, this river also served in generating hydroelectric power and has been providing water supply to the domestic and industrial utility of modern cities of South India. In the downstream of the Cauvery basin, rice is the major crop for which the region is known as the rice bowl of Tamil Nadu. Hence, the objectives of this paper are to identify the spatiotemporal shift of extreme droughts over time and to elucidate the variability of extreme drought indices over the Cauvery River basin.

Drought prediction generally refers to the prediction of droughts severity (e.g., values of a specific drought indicator). In some instances, drought prediction also relates to other properties, such as drought duration and frequency, or phases, such as drought onset, persistence, and recovery. In this study, we mainly focus on the progression of extreme droughts over time, their periodicities, and their association with SST.

Following the introduction section, data and study area details are presented in Sect. 2. Section 3 describes the methodology. Following that the results and discussion are presented in Sect. 4. The paper ends with concluding remarks.

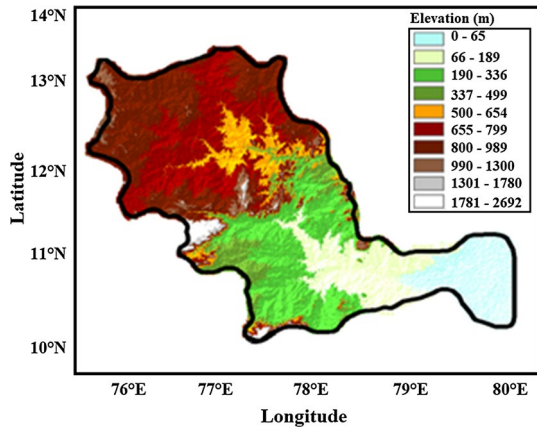
2 Study area

The Cauvery River originates from the Brahmagiri range of hills in the Western Ghats. It flows from west to east direction majorly covering the state of Karnataka, and Tamil Nadu and some part in Puducherry. The span of the river is about 800 km from its origin to outfall into the sea. While the majority of the river stretch lies in the state of Tamil Nadu (416 km), the river flows around 320 km in the state of Karnataka (Jain et al. 2007). The Cauvery River basin experiences tropical climate and is characterized by per humid, moist sub-humid, dry sub-humid, and semi-arid zones. While the southwest monsoon contributes 90% of rainfall (Gholami and Srikantaswamy 2009), the basin also receives a partial contribution of rain from North-East Monsoon that mostly happens in the region of Tamil Nadu. Over the area, the basin experiences 956 mm of average annual rainfall (Gosain et al. 2006) with large diurnal variation (varies in between 44 to 18 °C in temperature).

Physiographically, the basin is composed of three parts, namely—the Western Ghats, the Plateau of Mysore, and the Delta. The delta area is the utmost agricultural productive zone in the basin. The significant portion of the basin is enclosed with agricultural land accounting for 66.21% of the total area.

Geographically, it stretches from the longitude 75.25°–79.25° degree east and latitude range from 10.25° to 13.25° degree north, which is shown in Fig. 1. The total area covered by the basin is comprised of 116 grids with a spatial resolution of 0.25° × 0.25° (approximately 27.85 km²).

Fig. 1 Geographical map of the Cauvery river basin



3 Data and methodology

3.1 Data description

This paper used monthly gridded rainfall data of resolution $0.25^\circ \times 0.25^\circ$ obtained from the Indian Institute of Tropical Meteorology (IITM), Pune (<http://www.tropmet.res.in>) spanning from 1931 to 2010. The data can be downloaded using the below link: (http://www.imdpune.gov.in/Clim_Pred_LRF_New/Gridded_Data_Download.html). Further, to analyze the effect of global warming over the region, two non-overlapping datasets have been prepared. The first dataset (i.e., rainfall and temperature) ranging from 1931 to 1970, known as pre-era of global warming, and the second dataset spanning from 1971 to 2010 is the post-era of global warming. The quality of data has been verified in several case studies both on the local scale and the entire region of India (Pai et al. 2014, 2017). The drought induced by the evapotranspiration is analyzed by utilizing the potential evapotranspiration (PET) data, obtained from the open web repository of Climate Research Unit, UK (CRU) <http://www.cru.uea.ac.uk>, spanning over the period 1931–2010 with $0.50^\circ \times 0.50^\circ$ resolution (Harris et al. 2014). To perform the complete analyses, the data of PET are rescaled to $0.25^\circ \times 0.25^\circ$ (same as the spatial resolution of rainfall data) using bilinear interpolation. Further, to visualize/explore the relationship between drought indices at different scales with sea surface temperature, the extended reconstructed sea surface temperature (ERSST) dataset is utilized from 1931 to 2005 at a monthly scale. This dataset is derived from the National Oceanic and Atmospheric Administration (NOAA) with missing data filled in by statistical methods.

3.2 Methodology

The methods used in the paper are presented in a schematic in Fig. 2. As shown in Fig. 2, the present study includes three methods for the analysis, in which SPI, SPEI, and CWT are utilized for the extraction of spatiotemporal characteristics of extreme droughts. For SPI, monthly rainfall data are taken as input, whereas the SPEI takes both PET and rainfall for the calculation of indices. Further, the count of extreme droughts obtained from SPI/SPEI over time is used to extract the significant periodicities over the river basin. For this

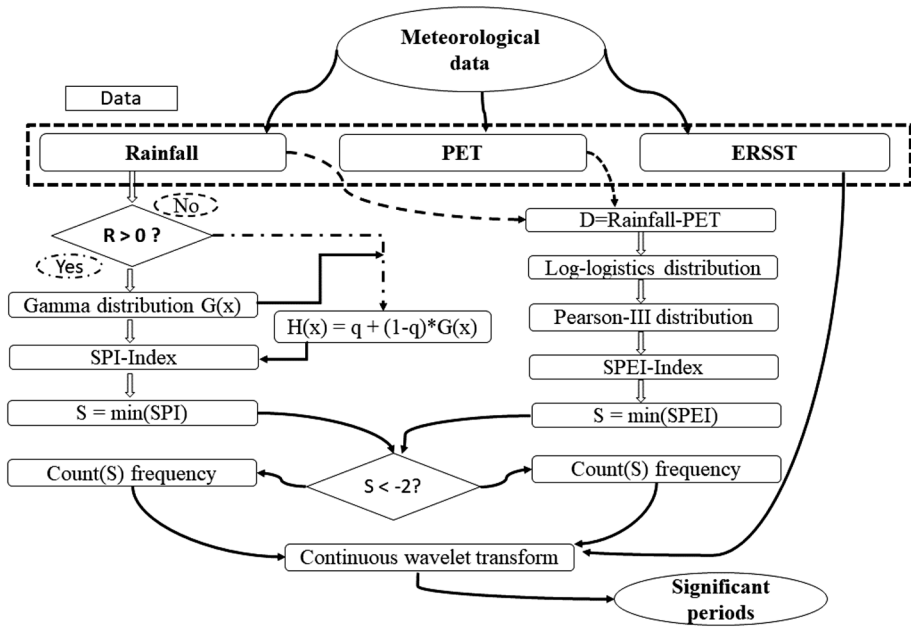


Fig. 2 Schematic of methods of SPI and SPEI

purpose, a continuous wavelet transform method is utilized. The details are summarized below:

3.2.1 SPI algorithm and interpretation

SPI is one of the widely used drought indices derived from rainfall deficiency. Typically, the SPI index is calculated for the selected time scales, i.e., 3-, 6-, 12-, and 24-month. The rainfall at time scales 3- and 6-month provides the information about the short-term droughts, whereas 12- and 24- month provide long-term droughts. The 3-month SPI negative index helps to identify the shortage of soil moisture, and it also includes information about the adequacy of precipitation of selected region through a positive index. The 6-month negative SPI index indicates a medium-range deficiency in the rain, and it mainly controls the streamflow and reservoir levels in the basin. Finally, long-term SPI negative indexes such as 12 and 24-month indicate the shortage in reservoir levels as well as groundwater levels (Belayneh et al. 2014). The monthly precipitation time series for j th time scale is modeled using gamma distribution (Thom 1958). The probability density function of the gamma distribution is defined by,

$$g(x) = \frac{1}{\beta^\alpha \Gamma(\alpha)} x^{\alpha-1} e^{-\frac{x}{\beta}} \quad \text{for } x > 0 \tag{1}$$

where $\alpha > 0$ is a shape parameter, $\beta > 0$ is a scale parameter, and $x > 0$ is the amount of precipitation. The parameters, such as α and β , are to be estimated for the fitting of distribution to data. These parameters are estimated for each time step of interest (3-, 6-, 12-, and 24-months). For this purpose, Edwards and McKee (1997) suggest that the maximum

likelihood estimator can be used for the estimation of these parameters (Thom 1958). It is obtained that

$$\hat{\alpha} = \frac{1}{4A} \left(1 + \sqrt{1 + \frac{4A}{3}} \right) \quad \text{and}$$

$$\hat{\beta} = \frac{\bar{x}}{\hat{\alpha}}$$

where $A = \ln(\bar{x}) - \frac{\sum \ln(x)}{n}$ and n is the number of precipitation observations. $\gamma(\alpha)$ is the gamma function, which is defined as:

$$\gamma(\alpha) = \int_0^\infty y^{\alpha-1} e^{-y} dy \tag{2}$$

By using the estimates of α and β , integrating the probability density function (Eq. 1) with respect to x yields an expression for the cumulative probability function of Gamma distribution is given by:

$$G = \int_0^x g(x) dx = \frac{1}{\beta^\alpha \gamma(\alpha)} \int_0^x x^{\alpha-1} e^{-\frac{x}{\beta}} dx \tag{3}$$

Since the gamma distribution is undefined for $x=0$, the cumulative distribution function for gamma distribution which accounts zero value in the data is further modified as:

$$H(x) = q + (1 - q)G(x) \tag{4}$$

where q is the probability of zero rainfall over time. The cumulative probability distribution obtained from Eqs. 3 and 4 is then transformed into standard normal distribution to yield the SPI, where positive values of the SPI indicate higher than mean precipitation, and negative values indicate less than mean precipitation. If the 3-month SPI for March 1995 is -2.00 , then the precipitation is much less than average compared to all other records of precipitation totals of March. When the 3-month SPI for March is $+1.00$, then the precipitation for the same month is substantially above average.

3.2.2 SPEI computation

SPEI computation requires two different datasets including monthly precipitation and PET. The PET data are computed based on the Thornthwaite method. Deficit or surplus accumulation of rainfall at different time scales (e.g., 3-, 6- month) is obtained by a simple arithmetic difference between precipitation, P and PET.

$$D_{ij}^k = P_{ij}^k - PET_{ij}^k \tag{5}$$

The difference D_{ij}^k in a given month j and year i depends on the chosen time scale k . For example, the accumulated difference for l month in a particular year i with a 12-month time scale is calculated using:

$$\begin{aligned}
 x_{i,j}^k &= \sum_{l=13-k+l}^{12} D_{i-1,l} + \sum_{l=1}^j D_l \quad \text{if } j < K \quad \text{and} \\
 x_{i,j}^k &= \sum_{l=j-k+1}^j D_{i,l} \quad \text{if } j > K
 \end{aligned}
 \tag{6}$$

where $D_{i,l}$ is the $P - PET$ difference in the first month of year i , in millimeters.

It is possible that D value could be negative when $P_i < PET_i$. In such a situation, a three-parameter distribution is needed to calculate the SPEI. Vicente-Serrano (2005) found the log-logistic distribution correlates best with the series compared with the other three selected three-parameter distributions such as Pearson III, lognormal, and general extreme values. Therefore, log-logistic probability density function was used to fit the data and the probability density function of log-logistic distribution (LLD) is expressed as:

$$f(x) = \frac{\beta}{\alpha} \left(\frac{x - \gamma}{\alpha} \right) \left[1 + \left(\frac{x - \gamma}{\alpha} \right) \right]^{-2}
 \tag{7}$$

where α , β , and γ are scale, shape, and origin parameters, respectively. The optimal estimation of three parameters of LLD can be obtained using which are obtained using the L-moment procedure is given below (Singh et al. 1993):

$$\begin{aligned}
 \beta &= \frac{2w_1 - w_0}{6w_1 - w_0 - 6w_2} \\
 \alpha &= \frac{(w_0 - 2w_1)\beta}{\gamma(1 + 1/\beta)\gamma(1 - 1/\beta)}
 \end{aligned}
 \tag{8}$$

$$\gamma = w_0 - \alpha\gamma(1 + 1/\beta)\gamma(1 - 1/\beta)$$

where $\gamma(1 + 1/\beta)$ is the gamma function of $(1 + 1/\beta)$, w_s is the probability-weighted moments (PWMs) of order s is given below:

$$w_s = \frac{1}{n} \sum_{i=1}^n \left(1 - \frac{j - 0.35}{n} \right)^s D_i
 \tag{9}$$

where n is the number of data points and j is the range of observations in increasing order. Thus, the cumulative distribution function of the D series is given by

$$F(x) = \left[1 + \left(\frac{\alpha}{x - \gamma} \right)^\beta \right]^{-1}
 \tag{10}$$

using $F(x)$, the SPEI can easily be obtained from the classical approximation of Abramowitz and Stegun (1965):

$$\text{SPEI} = w - \frac{c_0 + c_1w + c_2w^2}{1 + d_1w^1 + d_2w^2 + d_3w^3}
 \tag{11}$$

where $w = \sqrt{-2\log(P)}$ for $P \leq 0.5$ and P is the probability of exceeding a determination D value, and $P = 1 - F(x)$ if $P > 0.5$, then P is replaced by the $1 - P$ and the sign of the

resultant SPEI is reversed. The constants are $C_0=2.515517$, $C_1=0.802853$, $C_2=0.010328$, $d_1=1.432788$, $d_2=0.189269$, and $d_3=0.001308$. Similarly, SPEI is applied over the rainfall data at different time scales. The functionality of SPEI is the same as with SPI.

3.2.3 Continuous wavelet transform (CWT)

A wavelet is a function with zero mean, localized in both frequency and time. While various wavelet transforms functions exist in the literature, the Morlet wavelet has been frequently used and is defined as:

$$\Psi_0(\eta) = \pi^{-\frac{1}{4}} e^{i\omega_0\eta} e^{-\frac{\eta^2}{2}} \quad (12)$$

where ω_0 and η are the dimensionless frequency and time, respectively. For periodic feature extraction, it has been proved that the Morlet wavelet with ($\omega_0=6$) is a good choice as it provides the right balance between time and frequency localization (Grinsted et al. 2004). The idea behind the CWT is to apply the wavelet as a bandpass filter to the time series. Detailed documentation is available in Torrence and Compo (1998).

The statistical significance of wavelet power can be assessed through a first-order autoregressive (AR1) process. The Fourier power spectrum of an AR1 process with lag-1 autocorrelation α (Allen and Smith 1996) is given by

$$P_k = \frac{1 - \alpha^2}{|1 - \alpha e^{-2i\pi k}|^2} \quad (13)$$

4 Results and discussion

4.1 Climatology of mean JJAS rainfall at the basin scale

The climatological mean of JJAS annual rainfall in the Cauvery basin is 411 mm with a standard deviation of 82.41 mm from the data selected for the period 1931–2010. The impact of droughts is investigated by dividing the entire basin into two parts based on the elevation. Accordingly, the upstream and downstream of the basin comprise 61 and 55 grids, respectively. It is found that the long-term climatological mean of the annual JJAS rainfall in the upstream is approximately 513.13 mm with a standard deviation of 100.32 mm, which is much higher than the downstream mean 297.64 mm, standard deviation 78.98 mm. The relative increase in rainfall in the upstream region is mainly due to the influence of the Western Ghat's mountain range (Gunnell 1997). The reason for the less rain in downstream is attributed to the weakening strength of monsoon after traveling through the mountainous region.

The year 1970 has been witnessed as a mean change year in average temperature in India as well as over the globe (Narula et al. 2018). Moreover, some of the Indian subdivisions have experienced the worst drought conditions in 1972 (Parthasarathy et al. 1987), and most of the droughts have occurred during the post-era of global warming. For these reasons, the total period is divided into two non-overlapping time domains such as 1931–1970 and 1971–2010, each of 40 years, which is sufficient for the climatological study. The rationale to split the dataset into two parts is mainly to analyze the climate change influence on the spatiotemporal shift of drought over the basin.

Table 1 Criteria of drought classification

Drought magnitude	Criteria
Mild	$-1.0 < \text{SPI} < 0$
Moderate	$-1.5 < \text{SPI} \leq -1.0$
Severe	$-2.0 < \text{SPI} \leq -1.5$
Extreme	$\text{SPI} \leq -2.0$

Table 2 Frequency of extreme drought classification based on quartile estimation

Category	Range of frequency	Range of quartile (%)	Description
Class 0	0	0	No extreme drought
Class 1	[1, 3]	[1, 24]	Low frequency
Class 2	[4, 6]	[25, 49]	Medium frequency
Class 3	[7, 10]	[50, 74]	High frequency
Class 4	≥ 11	[75, 100]	Exceptional high frequency

The numbers in the second column represent the frequency of extreme drought

4.2 SPI and SPEI index at gridded scale

The rainfall data for the selected period (1931–2010) are used for the computation of SPI and SPEI to perform droughts analysis at all-India, and gridded scale (Pai et al. 2011, 2017; Preethi et al. 2019). The SPI/SPEI is calculated at the end of each month. The data set is updated in the sense that at each month a new value is determined from the previous i months. For example, SPI-3 is obtained as a moving sum of 3 months with a monthly step, in the sense that each month a new value is determined from the previous 3 months. For the calculation of SPI-3 for March, the rainfall data of January, February, and March have been considered and so forth. Subsequently, the SPI and SPEI are applied at each grid over the entire river basin at 3-, 6-, 12- and 24-month. However, the results of 3- and 12-month are presented here. The magnitude of droughts such as mild, moderate, severe, and extreme has been classified based on McKee et al. (1993), and the classification scheme mentioned in Table 1 is followed in the present work. It is to be noted that only the extreme droughts are considered for the present analysis.

The relative change in the frequency of extreme droughts is assessed by partitioning the data into two non-overlapping periods, such as 1931–1970 and 1971–2010. The total number of extreme droughts over each grid is defined as the count. Further, different classification schemes establish the magnitude of frequency (i.e., low, medium, high). The classification of the count of extreme droughts is statistically estimated and is presented in Table 2. A similar classification scheme is also used by Narula et al. (2018) to segregate low and high affected temperature hotspots. The frequency of extreme droughts at a 3-month scale for the SPI and SPEI is shown in Fig. 3 and Table 3. The spatial pattern of the SPI-3 in 1931–1970, and 1971–2010 is depicted in Fig. 3a and b, respectively. It is found that the extreme droughts of different frequencies classified as class 1, class 2, and class 3 spread over the region in 1931–1970. It may be noted that none of the class 3 extreme drought events in the downstream of the basin is found in 1931–1970. However, in the second period 1971–2010, a significant number of class 3 drought events and a very

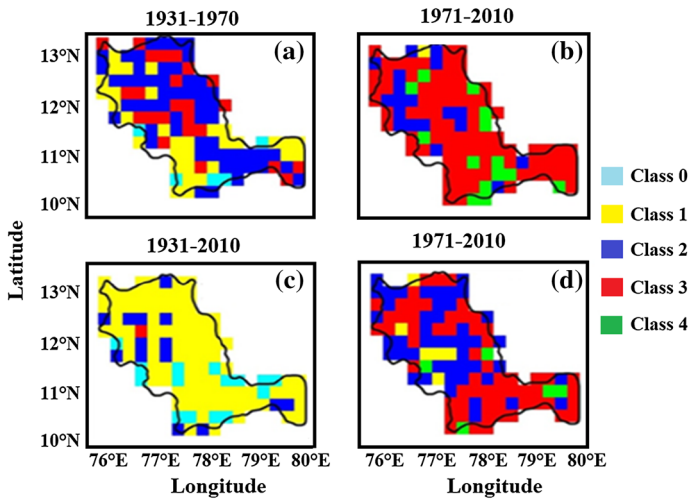


Fig. 3 Spatial distribution of frequency of the extreme droughts of SPI-3, and SPEI-3 over two non-overlapping time domains

Table 3 The classification of frequency of extreme drought of SPI-3, and SPEI-3

Class of extreme drought	1931–1970 (Percentage of grids) SPI	1971–2010 (Percentage of grids) SPI	SPEI (1931–1970)	SPEI (1971–2010)
Class 0	0	0	15 (13%)	0
Class 1	38 (33%)	1 (0.8%)	86 (74%)	6 (5%)
Class 2	54 (46%)	19 (16%)	14(12%)	46 (40%)
Class 3	24 (21%)	82 (71%)	1(0.8%)	64 (55%)
Class 4	0	14 (12%)	0	0

The numbers in the column represent the grids and its percentage of spatial distribution over the basin in two non-overlapping time domains

few class 4 drought events are found in 71% and 12% of basin area, respectively. These results suggest the progression of extreme drought events from low to high class is evident, as shown in Fig. 3. The progress of a 3-month extreme drought could adversely impact soil moisture; consequently, it negatively affects the vegetation and crop yields (Balasubramani 2006; Pangaluru et al. 2019; Rossato et al. 2017). Furthermore, short-term droughts might eventually lead to the development of long-term droughts. Mostly the effect of short drought conditions may not be visible in the long-term-scale drought.

Further, SPEI is implemented over grids, and extreme drought years are extracted using the Mckee et al. (1993) classification scheme. The frequency classification of extreme droughts is performed over each grid, and the results are illustrated in Fig. 3c, d. The results suggest that class 1 of extreme droughts is mainly found in 1931–1970 over the entire region wherein during 1971–2010 class 2 and class 3 are found to dominate over the basin. In turn, the influence of PET is found to be evident over the entire region in the second half of the total time. In the PET calculation, temperature plays a significant role; therefore, this might be due to a rapid increase in the maximum and minimum temperature

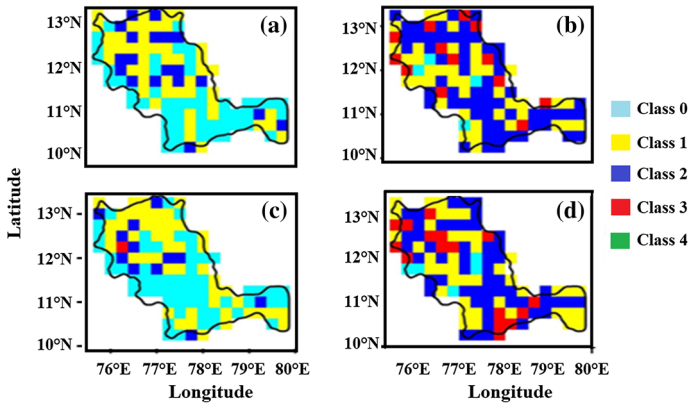


Fig. 4 Spatial distribution of frequency of the extreme droughts of SPI-12, and SPEI-12 over two non-overlapping time domains

Table 4 The classification of frequency of extreme drought of SPI-12, and SPEI-12

Class of extreme drought	1931–1970 (Percentage of grids) SPI	1971–2010 (Percentage of grids) SPI	SPEI (1931–1970)	SPEI (1971–2010)
Class 0	50 (43%)	4 (3%)	54 (46%)	5 (4%)
Class 1	47 (41%)	40 (34%)	47 (41%)	36 (31%)
Class 2	19 (16%)	59 (51%)	12 (10%)	53 (46%)
Class 3	0	13 (11%)	1 (0.8%)	16 (14%)
Class 4	0	0	0	0

The numbers in the column represent the grids and its percentage of spatial distribution over the basin in two non-overlapping time domains

over the southern part of India (Ross et al. 2018; Jain and Kumar 2012). It supports the fact that the influence of temperature intensifies the extreme drought condition over the region. Overall, it is observed that the progression of the frequency of extreme drought events is found over the area. In specific, the progression of the frequency of extreme drought events is very strong in the downstream region as compared to the upstream of the basin. These results suggest that in the recent past, the river basin experienced a significant reduction in the rainfall from normal events.

Similarly, extreme drought years are extracted at a 12-month scale. Accordingly, the indices SPI-12 and SPEI-12 are calculated for both periods, and the results are shown in Fig. 4 and Table 4. In which, the sub-plots, Fig. 4a, b, illustrate the spatial pattern of extreme droughts at a 12-month scale for both time domain (1931–1970 and 1971–2010). During the period 1931–1970, it is found that the class 0 of extreme droughts prevail over 43% area of the region, especially in the downstream of the basin. In contrast, the presence of class 0 is minimal in the upstream. It suggests that relatively a large area in the upstream suffers from the high frequency of extreme droughts as compared to downstream of the basin. Further, it is noticed that class 1 and class 2 cover 41% and 16% area of the region, respectively, in the first half of the period, whereas the spatial coverage of class 2 of extreme drought is increased by 300% in the second half. Especially, such progression of

extreme droughts is found in class 0 and class 2 in the downstream region, which suggests that the downstream of the basin experienced rapid growth of long scale extreme droughts. Furthermore, the results of SPEI-12 are depicted in Fig. 4c, d. The results suggest that class 0 (46%) and class 1 (41%) of extreme drought dominate over the whole river basin during the time 1931–1970. The presence of class 0 of extreme drought indicates the minimal effect of the PET and temperature. However, the maximal area coverage of a higher class of extreme drought indicates that the basin is highly affected by the rapid increase in temperature. This particular result supports the fact that in the recent past, the southern part of India experienced an increasing trend of average maximum, and minimum temperature (Jain and Kumar 2012). Moreover, the entire world is influenced by a rapid increase in annual average temperature after 1970 (global warming era) (Parker et al. 1995; Solanki and Krivova 2003). It is observed that during the period 1971–2010, most of the study region experienced extreme drought of class 2 and class 3. As long-term droughts have a direct impact on the reservoir storage, especially in the surface water scheme, improved reservoir operation policies are required to manage the water allocation.

4.3 Periodicity detection of the extreme drought years

The extreme drought years at each grid are calculated, and their count is obtained to identify further the probable existence of periodical changes over the basin from 1931 to 2010. For example, suppose 1905 is found to be an extreme drought year, and it occurred over 10 grids, then the count of 1905 would be 10. Further, CWT is implemented on the count of extreme drought years to extract useful information such as significant frequencies (1/period) concerning time (Torrence and Compo 1998). The map shown in Fig. 5 represents the normalized power spectrum of extreme drought years of SPI-3, and SPI-12 along with grid count of each year over the basin. These are obtained using Morlet wavelet where the contours represent a 95% confidence region. It can be deduced from Fig. 5a that significant periodicities in SPI-3 are seen in the band of 2, 2–3, 3.5–5, 9–14 years (y).

Further, the high periodicities in the 3–5 y and 9–14 y bands are found to be significant from 1992 to 2010, whereas small periodicities in the range of 2–3 y are noticed during 1935–1941 and 1980–1993. The existence of small periods in the band of 2–3 y might be the indication of more frequently repeating short-term droughts (3-month). It is also evident from Fig. 5b that most of the region (based on the grid count) have witnessed extreme droughts that occurred from 1934 to 1937, and 1975–2005. It is obtained that the extreme drought years at a 3-month scale of SPI have occurred over 79–97 grids during the period 2001–2002. Furthermore, the 58, 56, 51, and 50 grids have been affected by the droughts in 1937, 1991, 2000, and 1975, respectively. It indicates that the region suffered from extreme drought years mainly in the second half of the time domain. This further confirms the finding reported in the section of 4.2 that there is a transition of the low class of extreme droughts into high class in the second half time domain. Furthermore, at a 12-month scale, it is found that periods in the band of 3–4 and 4–12 y are significant over the region which is depicted in Fig. 5c. Also, it is seen that the high periodicities are significant from 1985 to 2010, whereas small periodicities are found to be significant during 1961–1965. It is also reported that ten El Nino events were observed during 1965–1998, which supports the dominant character of high periodicities in the extreme drought years (Dimri 2013; Yu et al. 2002). From Fig. 5d, it is observed that the extreme droughts occurred over the grids of 32, 28, 32, and 83 during 1961–1965, 1971–1978, 1988–1990, and 2000–2003, respectively.

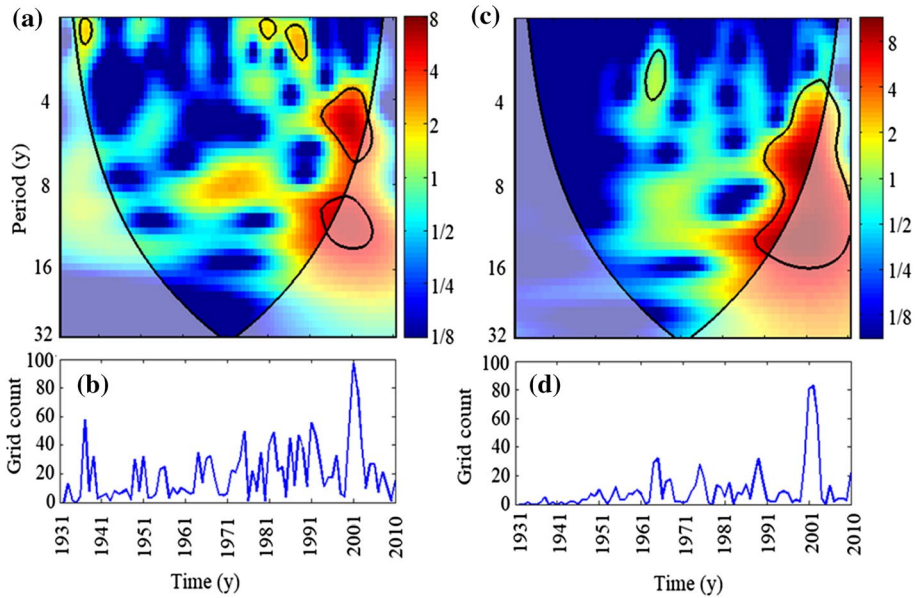


Fig. 5 Wavelet periodicity of the extreme drought years for **a** SPI-3; **b** grid count of extreme droughts years of SPI-3; **c** SPI-12; **d** grid count of extreme droughts years SPI-12. The 5% significance level against red noise is shown as a thick contour

From Fig. 5a c, it is observed that some common features exhibit between the dominant signal of SPI-3 and SPI-12 in the form of wavelet power. For example, the significant periodicities of both data series are found to be in 3.5–7, 9–14, and 3.5–12 y period band during the time domain of 1986–2010. Also, it is found that during 1961–2001 both series have high wavelet power in 7.5–10 y period band but are not significant at a 95% confidence level. In such cases, the existence of common significant periodicities becomes difficult to infer. For this purpose, wavelet coherence is very useful to extract the common significant periodicities and wavelet power. The results of the cross-wavelet spectrum of extreme drought years of SPI-3 and SPI-12 and their coherence are shown in Fig. 6a, b. It reveals that during 1986–2010, the dominant variability at the 4–12 y period band exhibits the highest wavelet power. Further, the right arrow sign in Fig. 6a represents an in-phase linkage between both the time series. The in-phase linkage of SPI-3 and SPI-12 from 1986 to 2010 further confirms the results as illustrated in Fig. 4. In-phase association between two signals leads to a high amplitude of the resultant signal. In this situation, the phase difference between two signals is either 0 or 2π . Hence, in-phase association of SPI-3 with SPE-12 is like to enhance the drought situation. Whereas in anti-phase, the phase difference between two signals is either π or 3π . In this situation, the amplitude of the resultant signal will be low. Hence, the effect of one signal may not be visible significant over the other signal. The interaction of two signals can be viewed as:

Let y_1 and y_2 be two signals are constructed as:

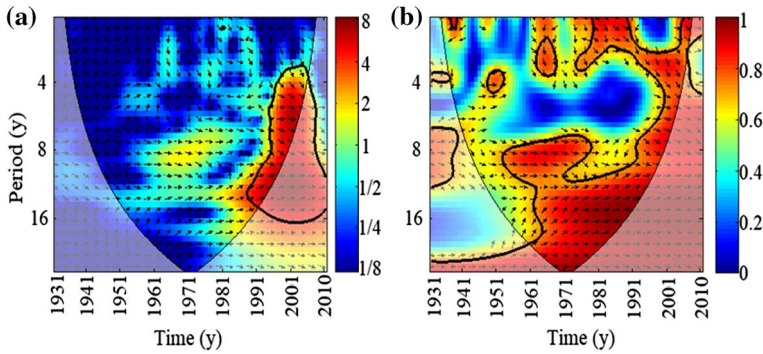


Fig. 6 **a** Cross-wavelet transforms of extreme drought years of SPI-3 and SPI-12; **b** wavelet coherence over the time domain 1931–2010. The 5% significance level against red noise is shown as a thick contour

$$y_1 = a_1 \sin(\omega_1 t + \omega_1)$$

$$y_2 = a_2 \sin(\omega_2 t + \omega_2)$$

where a_1 and a_2 are the amplitude of the two signals, ω_1 and ω_2 are two dominating frequencies, t is the period from 1901 to 2005.

$$I = a_1^2 + a_2^2 + 2a_1 a_2 \cos(d)$$

$$F = \sqrt{I}$$

$$d = t(\omega_1 - \omega_2) + (\varphi_1 - \varphi_2)$$

d is the phase difference over time. For $d=0, 2\pi$, the amplitude attains maximum, implies in-phase, whereas, for $d=\pi, 3\pi$, the amplitude attains minimum, implies anti-phase.

Similarly, the wavelet periodicities of the extreme drought years of SPEI-3 are obtained and are shown in Fig. 7a. It reveals that the 2–8 y period band exhibits the highest wavelet power which is significant during 1990–2005 and comparatively less wavelet power persists at a 2-y period band in 2000–2003. Further, the result reveals that extreme drought occurred in 1937, 1995, 1997, 2001, and 2003 spread over 49, 49, 91, 80, and 77 grids, respectively. As an increase in maximum and minimum temperature in the second half (1971–2010) has been evident, the entire basin has shown to have an elevated high frequent extreme drought. Also, similar results are obtained for SPEI-12, as presented in Fig. 7c, d. It may be concluded from Fig. 7d that during 2000–2003, the region has experienced deficit rainfall as well as a high rate of evapotranspiration due to positive changes in maximum and minimum temperature. Also, except in 1937, extreme drought years are found to be in the second half of the time domain, which further confirms the influence of the global warming effect on the basin. The cross-wavelet transforms, and coherence of SPEI-3 and SPEI-12 (figures are not shown here) reveal that from 1990 to 2005 both signals have significant periodicities in the 3–9 y period band and exhibit highest wavelet power. Further, it is observed that both the signals are associated with in-phase linkage. Wavelet coherence results suggest that during 1950–2000, the period band 7–14 y is linked in-phase, whereas the period band 2.5–6 y is linked with a lag of 90°. Furthermore, the 2–4 y period band is also connected with in-phase during 1945–1955.

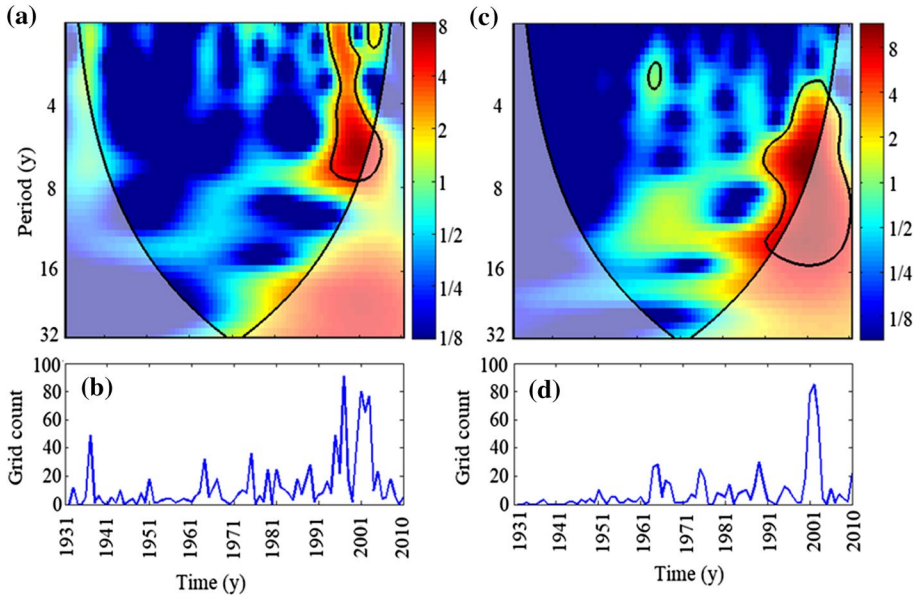


Fig. 7 Wavelet periodicities of the extreme drought years for **a** SPEI-3; **b** grid counts; **c** SPEI-12; and **d** grid counts. The 5% significance level against red noise is shown as a thick contour

4.4 The relation of drought variability with ERSST

To investigate the role of sea surface temperature (SST) in the formation of extreme drought at different time scales over the basin, ERSST of the annual data set is used. It is established in the literature that the ISMR is inversely correlated with ENSO (Rasmussen and Carpenter 1983; Sikka 1980; Pant and Parthasarathy 1981; Azad and Rajeevan 2016; Ihara et al. 2007). Further, an active spell of ENSO is indirectly responsible for forming drought over the globe, as well as in India (Kane 2004). This study additionally aims to establish a relation between the short-term and long-term droughts with SST. Therefore, to accomplish a fair comparison, the ERSST data are normalized concerning mean and standard deviation. Then, the significant periodicities of normalized ERSST and SPI-3 index are extracted using CWT. The results are shown in Fig. 8a, b. It is to be noted that the ERSST data are available only from 1931 to 2005. It is found that the variability of ERSST is contained within the year 2–4 y, 5–7 y, and 3–6 y period band and is not distributed uniformly over time. The significant periodicities of high wavelet power within the contour are time localized and noticed in 1985–2005 with 3–5 y cycle, whereas 2–4 and 5–7 y period bands are found in 1970–1980 and 1950–1960, respectively. Similarly, for the negative index of SPI-3, the significant periodicities are found during 1940 and 1990–2010 with the periodicities of 2- and 2–7 y, respectively as shown in Fig. 8b.

It is noticed that the negative index of SPI-3 and ERSST have dominant variability in 2–7 years period band which is significant during 1985–2005 (Fig. 8a, b). Further, it is observed that both time series have the highest wavelet power (i.e., 2–4 y band) in 1965–1975; however, only the ERSST has significant power at 95% confidence level (shown as a thick contour in Fig. 8a). In such cases, cross-wavelet and wavelet coherence help to identify the localized time and period band for which both time series have the

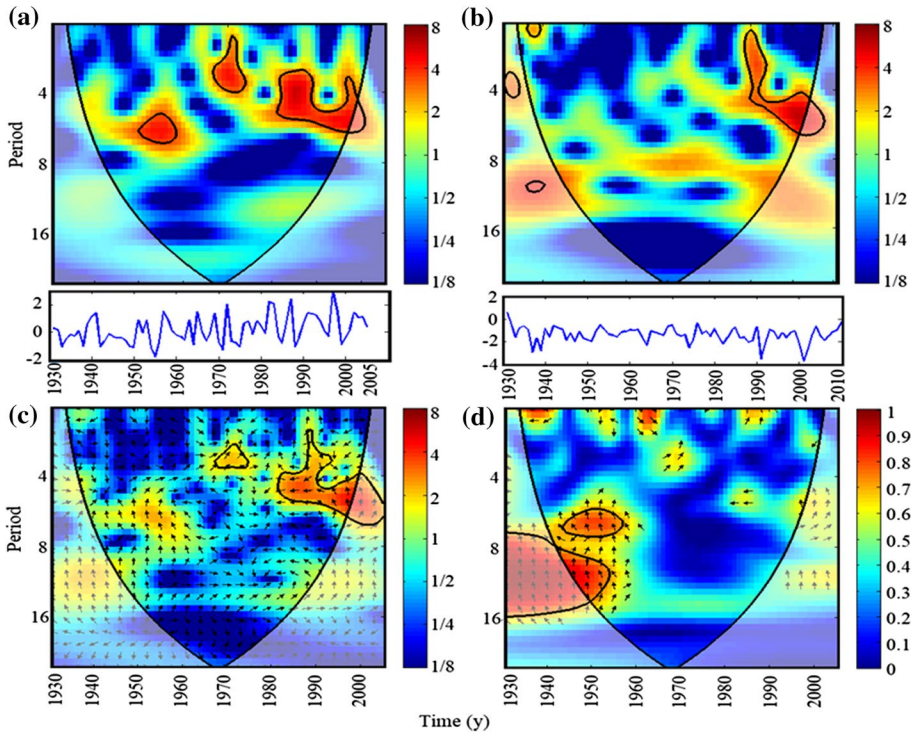


Fig. 8 Wavelet periodicities of **a** normalized ERSST index; **b** SPI-3; **c** for cross-wavelet transform of normalized ERSST index and SPI-3-negative index; **d** Squared wavelet coherence between them. The 5% significance level against red noise is shown as a thick contour

leading signals (i.e., dominant periodicity). Figure 8c, d represents the cross-wavelet and wavelet coherence of both time series. It reveals that significant periodicities of 2–4 y and 2–7 y period bands are found in 1945–1960, 1965–1975, and 1980–2005, respectively. Further, it indicates that the periodicities of both time series are associated with anti-phase during 1980–2005 and 1965–1975. The anti-phase association of two time series in the frequency domain reflects in the time domain. In this situation, the phase difference between two signals (SPI-3 and ERSST) is either π or 3π , and it leads to reduce the amplitude of the resultant signal. Thus, the ERSST and negative index of SPI-3 are negatively correlated in the time domain during the association period. Although the correlation coefficient (-0.2) is not significant, it is found to be connected with anti-phase relation in frequency domain.

Similarly, the significant periodicities of the 4–12 y period band are found in the negative index of SPI-12 during 1990–2010 (Fig. 9b). Also, other significant periodicities of 2–3 y band are noticed in 2000–2010. The cross-wavelet spectrum of SPI-12 and ERSST is shown in Fig. 9c. These results reveal that both time series have common wavelet power in 2–3 y, 3.5–6 y, and 5–7 y period band during the year 1970, 1980–1990, and 1990–2000, respectively. Further, the in-phase linkage between these series with a lag less than 90° over the significant period, bands are marked with a right tilted arrow (Fig. 9c). In this situation, the phase difference between two signals is either 0 or 2π . In-phase association between two signals leads to a high amplitude

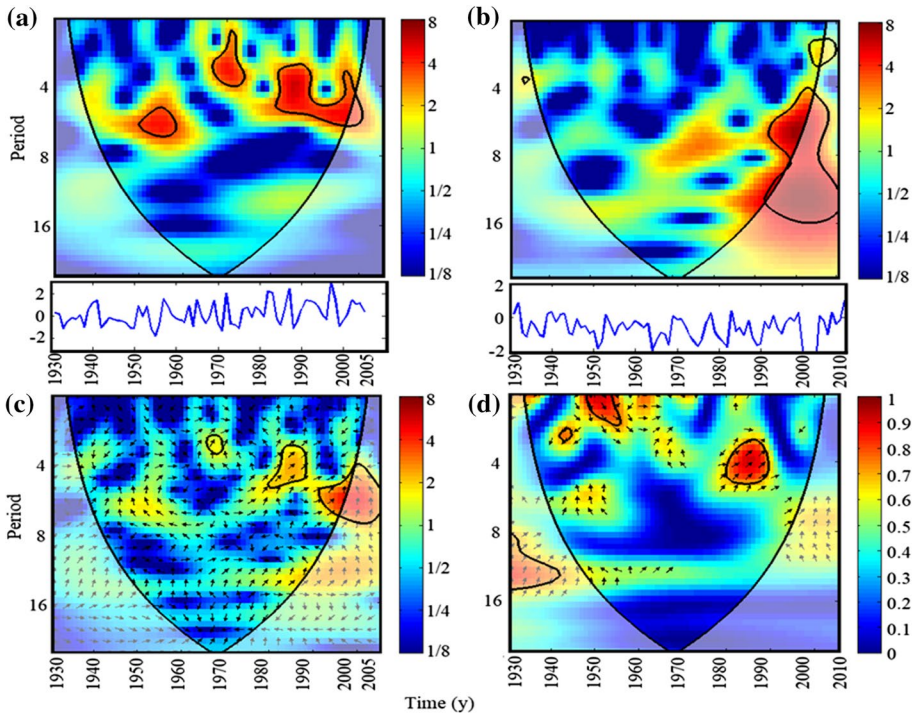


Fig. 9 a Wavelet periodicity of normalized ERSST index; b 12-month SPI; c for cross-wavelet transform of normalized ERSST index and 12-month SPI negative index; d Squared wavelet coherence between them. The 5% significance level against red noise is shown as a thick contour

of the resultant signal. Hence, in-phase association of SST with SPEI-12 is like to enhance the drought situation. These results further confirm the findings reported in Sect. 4.3 such that extreme drought events are very evident in most of the regions in 1980–2005. Further, the in-phase association in frequency domain reflects a positive correlation in the time domain between the selected time series over the significant period band.

Similar results are found in the wavelet power spectrum of SPEI-3 and SPEI-12 in 1931–2010 (figures are not shown). The significant variability at 2–3 and 5 y periodicities is seen in the negative index of SPEI-3 during 1990–2000, and 1995–2005, respectively. The cross-wavelet spectrum reveals the existence of common wavelet power at 2–3 and 5–7 y period band. Moreover, the periods of both time series are linked with a lag difference of 90° during 1995–2005 and in-phase relation during 1995–2000. The in-phase linkage further confirms the findings illustrated in Fig. 4 (i.e., the extreme droughts across the basin were very evident in 1995–2000). Therefore, the in-phase linkage suggests the intensified level of extreme drought conditions and it is reflected in Figs. 4 and 5. Similar observations are noted in the case of the negative index of SPEI-12, and the results are not presented here.

5 Summary and conclusions

Drought prediction is of critical importance to early warning for drought management. Since, drought events directly affect the water resources such as the dam reservoir, groundwater, and hence, the proper command is required. The presented results could be used for future planning and strategies. Further, it is crucial for water resource management and agricultural agencies to look at spatiotemporal characteristics of the droughts and their frequency, in specific to analyze the effect of extreme droughts over the Cauvery River basin. The proper management schemes will help to optimize the limited water resources of the river basin into diverse fields under the warming climate scenario. Furthermore, it is equally important to monitor the periodical behavior of such natural hazards for the benefit of socioeconomic development. Thus, this paper focused on examining changes in the frequency of extreme drought indices which are obtained from the deficit rainfall and PET at a river basin scale. The progression of low class to high-class extreme drought over two non-overlapping times is analyzed. From this, the significant periodicities are extracted for the selected periods to possibly identify the year that experiences small and long-term extreme drought. This will help policymakers and others to take proper action before the occurrence of such events. It is a known fact that climate is a complex phenomenon that is affected by some nonlinear driving forces in nature. The variability at a local scale is significantly associated with the nonlinear forcing such as SST. Thus, it is vital to find a possible link between them. The wavelet analysis of the SPI index at different scales predicts the possible occurrence of such events over time. The periodicities suggest that the extreme drought events are likely to occur over the region. The association with SST signifies that the relative strength of such a particular event. Suppose, SST and SPI-index have the same phase (in-phase), it is expected that the relative strength of the drought events would be more than in other cases.

The following conclusions are drawn from the above analysis.

1. The frequency of extreme droughts dominates in the second time domain (1971–2010) and found mainly in the downstream of the basin. In particular, the drought situation is found to be severe in 1975, 2002–2004, and the influence of temperature and PET is found to be extremely high during this period.
2. The entire river basin experienced a dominant cycle of 3.5–7 years of extreme droughts during the study period, and it is also found that extreme droughts were very prominent in 2000–2003.
3. The extreme droughts at a 3-month scale are influenced by biennial (2 y), quasi-biennial (2–3 y), and decadal oscillation, whereas ENSO and decadal oscillations modulate SPI-12.
4. The variability of ERSST is found to be contained within 2–4, 5–7, and 3–6 y period band. Whereas, SPI-3 and ERSST have a common periodicity in 2–4 and 2–7 y period band in the anti-phase.
5. The anti-phase association of the two (SPI-3 with ERSST) in frequency domain confirms the negative correlation during the association period. In contrast, a positive relationship is found between SPI-12 and ERSST having a lag of less than 90° .

Acknowledgements We are thankful to the Indian Institute of Tropical Meteorology, Pune for providing gridded data.

Author contributions KSK conceptualized the problem. PJ performed the experiments. PJ and KSK analyzed the data. PJ contributed reagents/materials/analysis tools. KSK, PJ, SA wrote the paper. PJ, KSK, SA contributed to the interpretation of results. PJ developed the codes.

References

- Abramowitz M, Stegun IA (1965) Handbook of Mathematical Functions, with Formulas, Graphs, and Mathematical Tables. Dover Publications, Washington DC
- Allen MR, Smith LA (1996) Monte Carlo SSA: detecting irregular oscillations in the presence of coloured noise. *J Clim* 9:3373–3404. [https://doi.org/10.1175/1520-0442\(1996\)009%3c3373:MCSDIO%3e2.0.CO;2](https://doi.org/10.1175/1520-0442(1996)009%3c3373:MCSDIO%3e2.0.CO;2)
- Arjun KM (2013) Indian agriculture-status, importance and role in Indian Economy. *IJAFST* 4(4):343–346
- Azad S, Rajeevan M (2016) Possible shift in the ENSO-Indian monsoon rainfall relationship under future global warming. *Sci Rep* 6:20145. <https://doi.org/10.1038/srep20145>
- Balasubramani KS (2006) Agricultural change and irrigation problem in the Cauvery Delta-Technological interventions and (NON) adoption processes. Doctoral dissertation, Indian Agricultural Research Institute, New Delhi
- Beguieria S, Vicente-Serrano SM, Martínez MA (2010) A multi-scalar global drought dataset: the SPEI base: a new gridded product for the analysis of drought variability and impacts. *Bull Am Meteorol Soc* 10:1351–1356
- Belayneh A, Adamowski J, Khalil B, Ozga-Zielinski B (2014) Long-term SPI drought forecasting in the Awash River Basin in Ethiopia using wavelet neural network and wavelet support vector regression models. *J Hydrol* 508:418–429. <https://doi.org/10.1016/j.jhydrol.2013.10.052>
- Cai W, Cowan T (2008) Evidence of impacts from rising temperature on inflows to the Murray-Darling Basin. *Geophys Res Lett*. <https://doi.org/10.1029/2008GL033390>
- Dimri AP (2013) Relationship between ENSO phases with Northwest India winter precipitation. *Int J Climatol* 33(8):1917–1923. <https://doi.org/10.1002/joc.3559>
- Dracup JA, Lee KS, Paulson EG (1980) On the statistical characteristics of drought events. *Water Resour Res* 16(2):289–296. <https://doi.org/10.1029/WR016i002p00289>
- Edwards DC, McKee TB (1997) Characteristics of 20th century drought in the United States at multiple time scales. *Climatology Rep.* 97–2, Department of Atmospheric Science, Colorado State University, Fort Collins, Colorado
- Fowler AM, Hennessy KJ (1995) Potential impacts of global warming on the frequency and magnitude of heavy precipitation. *Nat Hazards* 11(3):283–303
- Gao Y, Gao X, Zhang X (2017) The 2°C global temperature target and the evolution of the long-term goal of addressing climate change - from the United Nations framework convention on climate change to the Paris agreement. *Engineering* 3(2):272–278
- Gerten D, Rost S, von Bloh W, Lucht W (2008) Causes of change in 20th century global river discharge. *Geophys Res Lett*. <https://doi.org/10.1029/2008GL035258>
- Gholami S, Srikantaswamy S (2009) Analysis of agricultural impact on the Cauvery river water around KRS dam. *World Appl Sci J* 6(8):1157–1169
- Gosain AK, Rao S, Basuray D (2006) Climate change impact assessment on hydrology of Indian river basins. *Curr Sci* 90(3):346–353
- Grinsted A, Moore JC, Jevrejeva S (2004) Application of the cross wavelet transform and wavelet coherence to geophysical time series. *Nonlinear Process Geophys* 11(5–6):561–566
- Gunnell Y (1997) Relief and climate in South Asia: the influence of the Western Ghats on the current climate pattern of peninsular India. *Int J Climatol* 17(11):1169–1182. [https://doi.org/10.1002/\(SICI\)1097-0088\(199709\)17:11%3c1169:AID-JOC189%3e3.0.CO;2-W](https://doi.org/10.1002/(SICI)1097-0088(199709)17:11%3c1169:AID-JOC189%3e3.0.CO;2-W)
- Guttman NB (1998) Comparing the Palmer drought index and the standardized precipitation index. *J Am Water Resour AS* 34(1):113–121. <https://doi.org/10.1111/j.1752-1688.1998.tb05964.x>
- Harris IPDJ, Jones PD, Osborn TJ, Lister DH (2014) Updated high-resolution grids of monthly climatic observations—the CRU TS3.10 Dataset. *Int J Climatol* 34(3):623–642. <https://doi.org/10.1002/joc.3711>
- Hisdal H, Tallaksen LM (2003) Estimation of regional meteorological and hydrological drought characteristics: a case study for Denmark. *J Hydrol* 281(3):230–247. [https://doi.org/10.1016/S0022-1694\(03\)00233-6](https://doi.org/10.1016/S0022-1694(03)00233-6)
- Ihara C, Kushnir Y, Cane MA, Victor H (2007) Indian summer monsoon rainfall and its link with ENSO and Indian Ocean climate indices. *Int J Climatol* 27(2):179–187. <https://doi.org/10.1002/joc.1394>

- Intergovernmental Panel on Climate Change (IPCC) (2007) Climate Change 2007—Working Group I: the physical science basis. Cambridge University Press, Cambridge
- Jain SK, Kumar V (2012) Trend analysis of rainfall and temperature data for India. *Curr Sci* 102(1):37–49
- Jain SK, Agarwal PK, Singh VP (2007) Hydrology and water resources of India, vol 57. Springer, Berlin
- Jones P, Moberg A (2003) Hemispheric and large-scale surface air temperature variations: an extensive revision and an update to 2001. *J Clim* 16(2):206–223. [https://doi.org/10.1175/15200442\(2003\)016%3c0206:HALSSA%3e2.0.CO;2](https://doi.org/10.1175/15200442(2003)016%3c0206:HALSSA%3e2.0.CO;2)
- Kane RP (2004) Relation of El-Nino characteristics and timing with rainfall extremes in India and Australia. *Mausam* 55(2):257–268
- Kumar KN, Rajeevan M, Pai DS, Srivastava AK, Preethi B (2013) On the observed variability of monsoon droughts over India. *Weather and Climate Extremes* 1:42–50. <https://doi.org/10.1016/j.wace.2013.07.006>
- Logan KE, Brunell NA, Jones AR, Feddema JJ (2010) Assessing spatiotemporal variability of drought in the US central plains. *J Arid Environ* 74(2):247–255. <https://doi.org/10.1016/j.jaridenv.2009.08.008>
- Lorenzo-Lacruz J, Vicente-Serrano SM, López-Moreno JI, Beguería S, García-Ruiz JM, Cuadrat JM (2010) The impact of droughts and water management on various hydrological systems in the headwaters of the Tagus River (central Spain). *J Hydrol* 386(1–4):13–26. <https://doi.org/10.1016/j.jhydrol.2010.01.001>
- McKee TB, Doesken NJ, Kleist J (1993). The relationship of drought frequency and duration to time scales. In: Proceedings of the 8th conference on applied climatology, vol 17(22), pp 179–183
- Mishra AK, Singh VP (2010) A review of drought concepts. *J Hydrol* 391(1–2):202–216. <https://doi.org/10.1016/j.jhydrol.2010.07.012>
- Nalbantis I, Tsakiris G (2009) Assessment of hydrological drought revisited. *Water Resour Manag* 23:881–897. <https://doi.org/10.1007/s11269-008-9305-1>
- Narasimhan B, Srinivasan R (2005) Development and evaluation of Soil Moisture Deficit Index (SMDI) and Evapotranspiration Deficit Index (ETDI) for agricultural drought monitoring. *Agric Forest Meteorol* 133:69–88. <https://doi.org/10.1016/j.agrformet.2005.07.012>
- Narula P, Sarkar K, Azad S (2018) A functional evaluation of the spatiotemporal patterns of temperature change in India. *Int J Climatol* 38(1):264–271. <https://doi.org/10.1002/joc.5174>
- Nicholls N (2004) The changing nature of Australian droughts. *Clim Change* 63(3):323–336. <https://doi.org/10.1023/B:CLIM.0000018515.46344.6d>
- Obasi GOP (1994) WMO's role in the international decade for natural disaster reduction. *Bull Am Meteorol Soc* 75(9):1655–1662
- Pai DS, Sridhar L, Guhathakurta P, Hatwar HR (2011) District-wide drought climatology of the southwest monsoon season over India based on standardized precipitation index (SPI). *Nat Hazards* 59:1797–1813
- Pai DS, Sridhar L, Rajeevan M, Sreejith OP, Satbhai NS, Mukhopadhyay B (2014) Development of a new high spatial resolution (0.25 × 0.25) long period (1901–2010) daily gridded rainfall data set over India and its comparison with existing data sets over the region. *Mausam* 65(1):1–18
- Pai DS, Guhathakurta P, Kulkarni A, Rajeevan MN (2017) Variability of meteorological droughts over India. In: *Observed climate variability and change over the Indian region*. Springer, Singapore, pp 73–87
- Palmer WC (1965) *Meteorological drought*, vol 30. US Department of Commerce, Weather Bureau
- Pandey RP, Mishra SK, Singh R, Ramasastri KS (2008) Streamflow drought severity analysis of Betwa river system (India). *Water Resour Manag* 22(8):1127–1141. <https://doi.org/10.1007/s11269-007-9216-6>
- Pangaluru K, Velicogna I, Mohajerani Y, Ciraci E, Cpepa S, Basha G, Rao S (2019) Soil Moisture Variability in India: relationship of Land Surface-Atmosphere Fields Using Maximum Covariance Analysis. *Remote Sens* 11(3):335. <https://doi.org/10.3390/rs11030335>
- Pant GB, Parthasarathy SB (1981) Some aspects of an association between the southern oscillation and Indian summer monsoon. *Arch Meteorol Geophys Bio Climatol Ser B* 29:245–252. <https://doi.org/10.1007/bf02263246>
- Parker DE, Folland CK, Jackson M (1995) Marine surface temperature: observed variations and data requirements. *Clim Change* 31(2–4):559–600
- Parthasarathy B, Sontakke NA, Monot AA, Kothawale DR (1987) Droughts/floods in the summer monsoon season over different meteorological subdivisions of India for the period 1871–1984. *Int J Climatol* 7(1):57–70. <https://doi.org/10.1002/joc.3370070106>
- Preethi B, Ramya R, Patwardhan SK, Mujumdar M, Kripalani RH (2019) Variability of Indian summer monsoon droughts in CMIP5 climate models. *Clim Dyn* 53(3–4):1937–1962
- Rasmussen EM, Carpenter TH (1983) The relationship between eastern equatorial Pacific SST and rainfall over India and Sri Lanka. *Mon Weather Rev* 111:517–528

- Ross RS, Krishnamurti TN, Pattnaik S, Pai DS (2018) Decadal surface temperature trends in India based on a new high-resolution data set. *Sci Rep* 8(1):7452
- Rossato L, Marengo JA, Angelis CFD, Pires LBM, Mendiondo EM (2017) Impact of soil moisture over Palmer Drought Severity Index and its future projections in Brazil. *RBRH*. <https://doi.org/10.1590/2318-0331.0117160045>
- Sen Z (1980) Statistical analysis of hydrologic critical droughts. *J Hydraul Eng* 106(1):99–115
- Sikka DR (1980) Some aspects of the large scale fluctuations of summer monsoon rainfall over India in relation to fluctuations in the planetary and regional scale circulation parameters. *Proc Ind Acad Sci Earth Planet Sci* 89:179–195. <https://doi.org/10.1007/BF02913749>
- Singh VP, Guo H, Yu FX (1993) Parameter estimation for 3-parameter log-logistic distribution (LLD3) by Pome. *Stoch Hydrol Hydraul* 7(3):163–177
- Solanki SK, Krivova NA (2003) Can solar variability explain global warming since 1970? *J Geophys Res-Space*. <https://doi.org/10.1029/2002JA009753>
- Thom HC (1958) A note on the gamma distribution. *Mon Weather Rev* 86(4):117–122. [https://doi.org/10.1175/1520-0493\(1958\)086%3c0117:ANOTGD%3e2.0.CO;2](https://doi.org/10.1175/1520-0493(1958)086%3c0117:ANOTGD%3e2.0.CO;2)
- Torrence C, Compo GP (1998) A practical guide to wavelet analysis. *Bull Am Meteorol Soc* 79(1):61–78. [https://doi.org/10.1175/1520-0477\(1998\)079%3c0061:APGTWA%3e2.0.CO;2](https://doi.org/10.1175/1520-0477(1998)079%3c0061:APGTWA%3e2.0.CO;2)
- Tsakiris G, Pangalou D, Vangelis H (2007) Regional drought assessment based on the Reconnaissance Drought Index (RDI). *Water Resour Manag* 21(5):821–833. <https://doi.org/10.1007/s11269-006-9105-4>
- USDA (1994) Major world crop areas and climatic profiles, World Agricultural Outlook Board, US Department of Agriculture, Agricultural Handbook No 664: 157–70
- Vasiliades L, Loukas A, Liberis N (2011) A water balance derived drought index for Pinios River Basin. Greece. *Water Resour Manag* 25(4):1087–1101. <https://doi.org/10.1007/s11269-010-9665-1>
- Vicente-Serrano SM (2005) Differences in spatial patterns of drought on different time scales; an analysis of the Iberian Peninsula. *Water Resour Manag*. <https://doi.org/10.1007/s11269-006-2974-8>
- Vicente-Serrano SM, Beguería S, López-Moreno JI, Angulo M, El Kenawy A (2010a) A new global 0.5 gridded dataset (1901–2006) of a multiscalar drought index: comparison with current drought index datasets based on the Palmer Drought Severity Index. *J Hydrometeorol* 11(4):1033–1043. <https://doi.org/10.1175/2010JHM1224.1>
- Vicente-Serrano SM, Beguería S, López-Moreno JI (2010b) A multiscalar drought index sensitive to global warming: the standardized precipitation evapotranspiration index. *J Clim* 23:1696–1718. <https://doi.org/10.1175/2009JCLI2909.1>
- Xie SP, Deser C, Vecchi GA, Ma J, Teng H, Wittenberg AT (2010) Global warming pattern formation: sea surface temperature and rainfall. *J Clim* 23(4):966–986. <https://doi.org/10.1175/2009JCLI3329.1>
- Yu JY, Mechoso CR, McWilliams JC, Arakawa A (2002) Impacts of the Indian Ocean on the ENSO cycle. *Geophys Res Lett* 29(8):46-1. <https://doi.org/10.1029/2001GL014098>
- Zhang Q, Xu CY, Gemmer M, Chen YD, Liu CL (2008) Changing properties of precipitation concentration in the Pearl River basin, China. *Stoch Env Res Risk A* 23(3):377–385. <https://doi.org/10.1007/s00477-008-0225-7>